JOURNAL OF THERMOPHYSICS AND HEAT TRANSFER
Vol. 34, No. 1, January–March 2020

Heat Flux Data Reduction Using a Preconditioning Trial Function

J. I. Frankel* and Hongchu Chen†
University of Tennessee, Knoxville, Tennessee 37996-2210

DOI: 10.2514/1.T5744

This paper presents 1) a new preconditioned data reduction formulation, and 2) enhanced thin-film temperature gauge model for estimating the source heat flux applicable to impulsive test facilities used in hypersonic test programs. In such short-time tests, the heat flux is recovered from an active temperature-sensitive thin film. The physical situation permits a constant-property, semi-infinite substrate heat conduction model to be formulated relating the net substrate heat flux to the thin-film interface. Conventional lumped models assume no volumetric effects in the thin film. An enhanced boundary condition for the substrate is proposed that includes the storage of energy in the thin film. There are cases when the energy storage in the thin film should not be neglected. A parameter-free, physically motivated preconditioner is introduced to the integral equation system. This concept is applied to both the conventional and enhanced thermal models for predicting the source heat flux. A future-time method is proposed as the regularization scheme. The optimal future-time parameter is identified using a thermal phase-plane analysis that provides both a qualitative and quantitative means for estimating optimality. Highly favorable results are demonstrated for the simulated data sets based on a constant heat flux pulse.

Nomenclature

A_c = cross-sectional area, m^2
a = constant, $s^{-1/2}$
c = specific heat capacity, $J/(kg \cdot K)$
$\dot{E}$ = energy rate, W
k = thermal conductivity, $W/(m \cdot K)$
k_m = kernels with appropriate units
M_f = multiplication factor
M_m = kernels with appropriate units
N = number of data points beyond the initial condition
P = maximum number of future time parameters
q'' = heat flux, W/m^2
q_s'' = source heat source, W/m^2
$\tilde{q}''_{s,\gamma_n,N}$ = approximate source heat flux, W/m^2
R_q = cross-correlation coefficient for heat flux
$R_{\dot{q}}$ = cross-correlation coefficient for heat flux rate
$\Re$ = real part
T = temperature, °C
T_o = initial temperature, °C
t = time, s
$t_{\max}$ = maximum data collection time, s
u = dummy time variable, s
w = width of plate, m
x = spatial coordinate, m
z = dummy variable
α = thermal diffusivity, m^2/s
β = thermal effusivity, $W\sqrt{s}/(m^2 \cdot K)$
Δt = time sampling intervals, s
Δx = thickness of thin-film sensor, m
δ = Dirac delta function
η = constant, $\sqrt{s}$
γ = future time parameter, s
γ_n = future time parameter, s
ν_m = coefficient with appropriate units
θ = reduced temperature, $T - T_o$, °C
$\hat{\theta}_\lambda$ = Fourier transformed reduced temperature, $K \cdot m$
θ_f = film reduced temperature, °C
ρ = density, kg/m^3

Presented as Paper 2019-1553 at the AIAA SciTech Forum, San Diego, CA, 7–11 January 2019; received 17 February 2019; revision received 23 June 2019; accepted for publication 14 August 2019; published online 20 September 2019.

*Professor, Mechanical, Aerospace and Biomedical Engineering Department; jfranke1@utk.edu. Associate Fellow AIAA (Corresponding Author).
†Research Associate, Mechanical, Aerospace and Biomedical Engineering Department; hchen28@utk.edu.

I. Introduction

MANY aerospace engineering applications [1–4] require the prediction of a test article's surface heat flux or source heat flux based on either 1) local [5–9] or global [10–18] surface temperature or 2) in-depth or backside temperature [19–29] measurements. The use of the latter measurement location leads to the so-called inverse heat conduction problem (IHCP), which is highly ill-posed [19,20]. In many applications involving surface temperature measurement, the fundamental measurement equation for producing the net surface heat flux is based on the exact solution of the linear heat equation [30] that presumes that all thermophysical properties are constant. This assumption could restrict the temperature range for its applicability especially in long-duration ground tests. Measurement techniques include null-point calorimetry [31,32], temperature-sensitive paints (TSP's) [10–18], and co-axial thermocouples [5–9]. When using an in-depth temperature sensor, a second inverse problem exists as the sensor itself does not represent the positional temperature described by the heat equation. In most studies, the in-depth thermocouple temperature is assumed to be the positional temperature necessitated by the heat equation [30]. Not accounting for this second inverse probe problem may lead to misleading (attenuated and delayed) surface heat flux results [33,34]. With regard to the IHCP, two approaches are presently being used in practice. The classical or "parameter required" [19,20] approach requires the specification of the host material's thermophysical properties, probe location, and probe characteristics (e.g., time constant). In contrast, a calibration approach is termed a "parameter-free" method [21–29] as the geometrical, thermophysical, and sensor characteristics are not explicitly stated in the measurement equation but are contained in the calibration data used in the formulation.

This paper focuses on improving data reduction associated with estimating the source heat flux from a thin-film temperature sensor [35–40]. Section II presents the two mathematical models to be examined: the conventional model and the enhanced model. Section III introduces a preconditioner that will be applied to each model and compared with the original integral model. It will be demonstrated that the chosen preconditioner is based on a step response function (not impulse response function). Section IV describes the inverse approach taken whereby a future-time regularization method is introduced into the ill-posed mathematical setting. A discrete and finite set of regularization parameters are used for producing a family of corresponding predictions. The optimal

regularization parameter is extracted using a thermal phase-plane concept and cross-correlation principles. Section V presents numerical results indicating the merit of the proposed preconditioner-regularization method for extracting the "best" source heat flux prediction. Section VI closes the paper with concluding remarks.

II. Formulation

Two thin-film heat transfer models describing the thin-film/substrate interaction are schematically displayed in Fig. 1. Both models assume that 1) the time frame is sufficiently small that the backside of the substrate remains at the initial condition; 2) one-dimensional heat conduction is dominant; and 3) constant thermophysical properties are applicable due to the relatively small temperature rise in the substrate. It is assumed throughout this paper that the cross-sectional area of the thin film is identical to the cross-sectional area of the substrate [35]. Further, it is assumed that there is no interpenetration of the thin film into the substrate during the manufacturing process. Thus, a sharp interface and perfect thermal contact are assumed between the thin film and substrate. In each case shown in Fig. 1, a general energy balance about the thin film's control volume (C.V.) can be express as

$$\dot{E}_{\text{in}} + \dot{E}_{\text{generated}} = \dot{E}_{\text{out}} + \dot{E}_{\text{storage}} \tag{1}$$

Figure 1a displays the schematic of the thin film/substrate omitting volumetric sources $\dot{E}_{\text{generated}} = \dot{E}_{\text{storage}} = 0$. Figure 1b displays a control volume (C.V.) that neglects self-heating ($\dot{E}_{\text{generated}} = 0$) effects but retains the storage of energy ($\dot{E}_{\text{storage}} \neq 0$). Normally, the thickness of the thin film is in the range of 0.1–2 μm for a rapid response and durability. The location of the y axis is indicative of volumetric effects in the lumped thin-film sensor. That is, $\Delta x = 0$ in Fig. 1a, whereas $|\Delta x| > 0$ in Fig. 1b. Notice that the net surface heat flux into each substrate defines the location of $x = 0$. The conventional model displayed in Fig. 1a will be referred to as model 1, and the enhanced model given in Fig. 1b will be referred to as model 2. Model 2 allows for a nonnegligible sensor thickness to be assumed (accounting for delay and attenuation effects due to the sensor itself).

A. Heat Conduction into the Substrate

The defined location of the x axis in Fig. 1 permits the following formulation for heat conduction into the substrate. The linear heat equation for a semi-infinite medium is [30]

$$\frac{1}{\alpha}\frac{\partial\theta}{\partial t}(x,t) = \frac{\partial^2\theta}{\partial x^2}(x,t), \qquad x \in [0,\infty), \qquad t \geq 0 \tag{2a}$$

where the reduced temperature is given as $\theta(x,t) = T(x,t) - T_o$; the spatial and temporal time variables are x and t, respectively; and the thermal diffusivity is α. Equation (2a) is subject, for the present study due to convenience, to the boundary conditions

$$q''(0,t) = -k\frac{\partial\theta}{\partial x}(0,t), \qquad t > 0 \tag{2b}$$

$$\lim_{x\to\infty}\theta(x,t) = 0, \qquad t > 0 \tag{2c}$$

where $q''(0,t)$ is the net (conductive) heat flux into the substrate, and k is the thermal conductivity. Further discussion on Eq. (2b) will be forthcoming. The initial condition is given by

$$\theta(x,0) = 0, \qquad x \geq 0 \tag{2d}$$

The analytic solution for the direct or forward problem is obtained by the Fourier cosine transform [41]. The transform pair is defined as ([41] p. 17).

Transform:

$$\hat{\theta}_\lambda(t) = \sqrt{\frac{2}{\pi}}\int_{x=0}^{\infty}\theta(x,t)\cos(\lambda x)\,\mathrm{d}x, \qquad (\lambda,t) \geq 0 \tag{3a}$$

Inversion:

$$\theta(x,t) = \sqrt{\frac{2}{\pi}}\int_{\lambda=0}^{\infty}\hat{\theta}_\lambda(t)\cos(\lambda x)\,\mathrm{d}\lambda \qquad (x,t) \geq 0 \tag{3b}$$

The solution readily becomes

$$\theta(x,t) = \frac{1}{\beta\sqrt{\pi}}\int_{u=0}^{t} q''(0,u)\frac{e^{-x^2/(4\alpha(t-u))}}{\sqrt{t-u}}\,\mathrm{d}u, \qquad (x,t) \geq 0 \tag{3c}$$

where $\beta = \sqrt{\rho c k}$ is the thermal effusivity or so-called thermal product of the substrate material, where c is the substrate's specific heat capacity and ρ is the substrate's density.

Equation (3c), evaluated at $x = 0$, becomes the *data reduction equation* for recovering the net surface heat flux, $q''(0,t)$ when a surface temperature, and $T(0,t)$ is known corresponding to the model described in Fig. 1a. Evaluating Eq. (3c) at $x = 0$ produces the first-kind Abel integral equation for net surface heat flux, $q''(0,t)$

$$\theta(0,t) = \frac{1}{\beta\sqrt{\pi}}\int_{u=0}^{t} q''(0,u)k_1(t-u)\,\mathrm{d}u, \qquad t \geq 0 \tag{4a}$$

where the convolution (or displacement) kernel, $k_1(t-u)$ is given as

$$k_1(t-u) = \frac{1}{\sqrt{t-u}}, \qquad t-u > 0 \tag{4b}$$

Owing to the location of the x axis defined in Fig. 1, this statement holds true for both models. The purpose of this formulation is stated

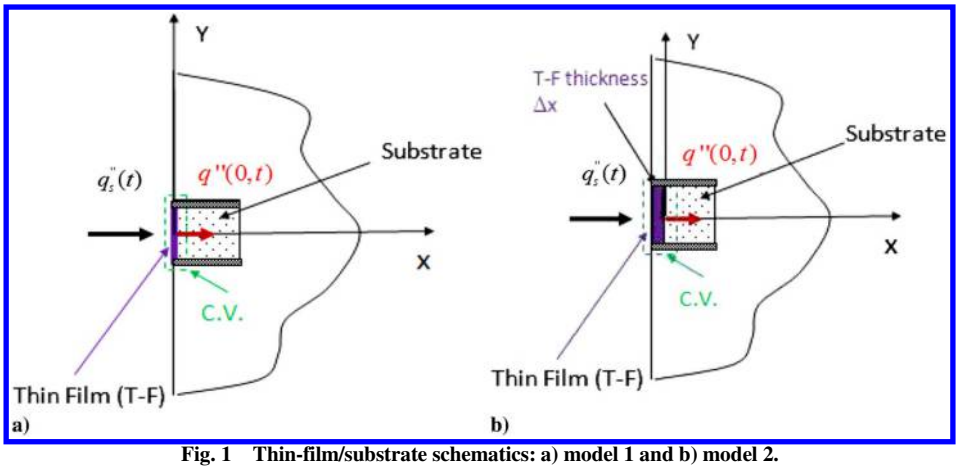

Fig. 1 Thin-film/substrate schematics: a) model 1 and b) model 2.

as "Given $\theta(0, t)$ determine $q_s''(t)$". When noisy data are present, ill-posedness is revealed as the sampling rate increases.

Inversion of Eq. (4a) can be accomplished in several ways and provides insight into the preconditioning process. Using a classical integral equation approach ([42] p. 47) and recognizing that Eq. (4a) is an Abel integral equation of the first kind permits inversion via the first iterate kernel leading to

$$q''(0,t) = \frac{\beta}{\sqrt{\pi}} \int_{z=0}^{t} \frac{\partial \theta}{\partial u}(0,u) k_1(t-u)\,\mathrm{d}u \qquad t \geq 0 \tag{4c}$$

An alternative formulation for Eq. (4c) is given by

$$q''(0,t) = -\frac{\beta}{\sqrt{4\pi}} \int_{u=0}^{t} \frac{\theta(0,u)}{(t-u)^{3/2}}\,\mathrm{d}u, \qquad t \geq 0 \tag{4d}$$

Equation (4d) can be arrived at by several approaches. Equation (4d) is the normal starting point for developing the Cook–Felderman discretization [43] often used in null point calorimetry [32], thin films [35], and co-axial thermocouples [44]. The Cook–Felderman discretization [43] is merely a discretization and does not address the ill-posedness of the formulation. Equations (4c) and (4d) describe heat flux in an explicit form that is commonly used [45] in experimental studies.

B. Model 1: Source Heat Flux, $q_s''(t)$

The control volume defined in Fig. 1a reduces the energy balance (W) in the thin film displayed in Eq. (1) to

$$\dot{E}_{\text{in}} = \dot{E}_{\text{out}} \tag{5a}$$

or in terms of the desired outcomes

$$q_s''(t)A_c = q''(0,t)A_c, \qquad t \geq 0 \tag{5b}$$

where A_c is the cross sectional area of the sensor. Substituting Eq. (4c) into Eq. (5b) produces the explicit form

$$q_s''(t) = \frac{\beta}{\sqrt{\pi}} \int_{z=0}^{t} \frac{\partial \theta}{\partial u}(0,u) k_1(t-u)\,\mathrm{d}u \qquad t \geq 0 \tag{5c}$$

In contrast, an implicit form is obtained by substituting Eq. (5b) into Eq. (4a) to arrive at

$$\theta(0,t) = \frac{1}{\beta\sqrt{\pi}} \int_{u=0}^{t} q_s''(u) k_1(t-u)\,\mathrm{d}u, \qquad t \geq 0 \tag{5d}$$

In fact, the latter relationship is the preferred formulation for this study.

C. Model 2: Source Heat Flux, $q_s''(t)$

The control volume defined in Fig. 1b reduces the energy balance (W) displayed in Eq. (1) to

$$\dot{E}_{\text{in}} = \dot{E}_{\text{out}} + \dot{E}_{\text{storage}} \tag{6a}$$

or in terms of the desired outcomes

$$q_s''(t)A_c = q''(0,t)A_c + (\rho c \Delta x)_f A_c \frac{\mathrm{d}\theta_f}{\mathrm{d}t}(t), \qquad t \geq 0 \tag{6b}$$

where $\theta_f(t)$ is the lumped, thin-film reduced temperature and $(\rho c \Delta x)_f$ is associated with the thermophysical and geometrical properties of the thin film. For the linear formulation, $\theta_f(t)$ represents the average temperature in the film. It should be noted that the heating rate $\mathrm{d}\theta_f/\mathrm{d}t$ can exceed 150,000 K/s in shock studies, and stating "thinness" as a rationale for omitting the storage term is insufficient. The storage term must be much smaller than the source term in these short-time studies. The initial temperature in the thin film and substrate is assumed identical. This formulation assumes the validity of a lumped thin-film analysis and the existence of ideal (perfect) interfacial contact between the thin film and substrate. The ideal thermal contact condition is expressed as

$$\theta_f(t) = \theta(0,t), \qquad t \geq 0 \tag{6c}$$

which permits Eq. (6b) to be written as

$$q_s''(t)A_c = q''(0,t)A_c + (\rho c \Delta x)_f A_c \frac{\partial \theta}{\partial t}(0,t), \qquad t \geq 0 \tag{6d}$$

Dividing Eq. (6d) by the cross-sectional area, A_c; solving for the net surface heat flux, $q''(0,t)$; and then substituting this result into Eq. (4a) produces

$$\theta(0,t) = \frac{1}{\beta\sqrt{\pi}} \int_{u=0}^{t} \left(q_s''(u) - (\rho c \Delta x)_f \frac{\partial \theta}{\partial u}(0,u) \right) k_1(t-u)\,\mathrm{d}u, \quad t \geq 0 \tag{6e}$$

This formulation is not convenient owing to the appearance of time derivative of the reduced surface temperature.

If given $q_s''(t)$ then Eq. (6e) can be viewed as an integro-differential equation for the reduced surface temperature, $\theta(0,t)$. However, the reverse is proposed for this study; that is, Eq. (6e) represents a Volterra integral equation of the first kind for the unknown source heat flux, $q_s''(t)$. Before proceeding further, it is advantageous to develop a standard form for future analysis. With this said, and Eq. (6e) being a linear functional equation, one can initially solve for the reduced surface temperature, $\theta(0,t)$, in terms of source heat flux, $q_s''(t)$, by Laplace transforms. Taking the Laplace transform of Eq. (6e) yields

$$L\{\theta(0,t)\} = \frac{1}{\beta\sqrt{\pi}} L\left\{ \int_{u=0}^{t} \left(q_s''(u) - (\rho c \Delta x)_f \frac{\partial \theta}{\partial u}(0,u) \right) k_1(t-u)\,\mathrm{d}u \right\}, \quad \Re(s) > 0 \tag{6f}$$

where L is the Laplace operator defined through ([46] p. 1020)

$$L\{f(t)\} = \hat{f}(s) = \int_{t=0}^{\infty} f(t) e^{-st}\,\mathrm{d}t, \qquad \Re(s) > 0 \tag{6g}$$

and possesses the convolution integral defined by ([46] p. 1020)

$$L\left\{ \int_{t=0}^{\infty} f(t) g(t)\,\mathrm{d}t \right\} = \hat{f}(s)\hat{g}(s), \qquad \Re(s) > 0 \tag{6h}$$

where $f(t)$ and $g(t)$ are real-valued functions.

With these definitions, Eq. (6f) becomes

$$\hat{\theta}(0,s) = \frac{1}{\beta\eta} \hat{q}_s''(s) \frac{1}{\sqrt{s}(\sqrt{s}+a)}, \qquad \Re(s) > 0 \tag{7a}$$

where $a = 1/\eta$ and $\eta = (\rho c \Delta x)_f/\beta$. Inverting Eq. (7a) ([46] p. 1024) through the convolution theorem produces

$$\theta(0,t) = \frac{1}{\beta\eta} \int_{u=0}^{t} q_s''(u) k_2(t-u)\,\mathrm{d}u, \qquad t \geq 0 \tag{7b}$$

where the kernel $k_2(t-u)$ is given as

$$k_2(t-u) = e^{a^2(t-u)} \operatorname{erfc}(a\sqrt{t-u}), \qquad t-u \geq 0 \tag{7c}$$

and where $\operatorname{erfc}(z)$ is the complementary error function ([46] p. 297).

A standardized form is now available for models 1 and 2, and can be written as

$$\theta(0,t) = \nu_m \int_{u=0}^{t} q_s''(u) k_m(t-u)\,\mathrm{d}u, \qquad m = 1,2, \qquad t \geq 0 \tag{8}$$

where $\nu_1 = (\beta\sqrt{\pi})^{-1}$ and $\nu_2 = (\beta\eta)^{-1}$. Here, $m = 1$ refers to model 1, and $m = 2$ refers to model 2.

Before departing this section, let us explicitly express Eq. (7b) as

$$\theta(0,t) = \frac{1}{(\rho c \Delta x)_f} \int_{u=0}^{t} q_s''(u) e^{\beta^2(t-u)/(\rho c \Delta x)_f^2} \times \operatorname{erfc}\left(\frac{\beta}{(\rho c \Delta x)_f}\sqrt{t-u}\right)\mathrm{d}u, \qquad t \geq 0 \tag{9}$$

Appendix A shows that Eq. (7b) properly reduces to Eq. (4a) as $\Delta x \to 0$ through a brief asymptotic analysis.

III. Physics-Based Preconditioning with Parameter-Free Function

A new data reduction methodology will be demonstrated and applied to the two previously developed models. The advantage of the new data reduction methodology will become self-apparent during the discussion. By expressing the models in a common form, it is possible to develop the preconditioner concept on Eq. (8) with the understanding that the coefficient ν_m and convolution (or displacement) kernel $k_m(t-u)$ take on the chosen model particulars. Additionally, a single numerical algorithm can be developed as the entire process is expressed in a standardized form applicable to both models and both data reduction schemes.

A. Time Domain Analysis

Let $t \to z$ in Eq. (8) to obtain

$$\theta(0,z) = \nu_m \int_{u=0}^{z} q_s''(u) k_m(z-u)\,\mathrm{d}u, \qquad m = 1,2, \qquad z \geq 0 \tag{10a}$$

Next, operate on Eq. (10a) with the trial function $\Psi_f(t-z)$ and integrate from $z = 0$ to $z = t$ to get

$$\int_{z=0}^{t} \Psi_f(t-z)\theta(0,z)\,\mathrm{d}z = \nu_m \int_{z=0}^{t} \Psi_f(t-z) \times \int_{u=0}^{z} q_s''(u) k_m(z-u)\,\mathrm{d}u\,\mathrm{d}z, \qquad m = 1,2, \qquad z \geq 0 \tag{10b}$$

Interchanging orders of integration on the right-hand side term in Eq. (10b) produces

$$\int_{z=0}^{t} \Psi_f(t-z)\theta(0,z)\,\mathrm{d}z = \nu_m \int_{u=0}^{t} q_s''(u) \times \int_{z=u}^{t} \Psi_f(t-z) k_m(z-u)\,\mathrm{d}z\,\mathrm{d}u, \quad m = 1,2, \quad z \geq 0 \tag{10c}$$

or in the standard form (let $z \to u$ on left-hand side for cosmetic reasons)

$$\int_{u=0}^{t} \Psi_f(t-u)\theta(0,u)\,\mathrm{d}u = \nu_m \int_{u=0}^{t} q_s''(u) M_m(t-u)\,\mathrm{d}u, \quad m = 1,2, \qquad z \geq 0 \tag{10d}$$

where

$$M_m(t-u) = \int_{z=u}^{t} \Psi_f(t-z) k_m(z-u)\,\mathrm{d}z, \quad m = 1,2, \qquad t-u \geq 0 \tag{10e}$$

One interpretation of this process is associated with a filtering operation of the functional equation. In many studies, a digital filter is applied solely on the raw reduced temperature data. This one-sided operation removes the equal sign from the energy balance. Further, ill-posed problems are highly sensitive to noise and the system's interpretation of noise. In an analytic setting, Eq. (10d) is equivalent to Eq. (10a). However, for an ill-posed setting involving noisy and discrete data, this approach could have a profound effect on outcomes.

Observations: 1) The function $\Psi_f(t)$ is reminiscent of a filter and hence should behave as a low-pass filter; b) if $\Psi_f(t) = \delta(t)$ then Eq. (10d) recovers Eq. (4a); c) if $q_s''(t) = \delta(t)$ then $\nu_m k_m(t)$ can be interpret as an impulse response function; and d) if $q_s''(t) = H(t)$ then $\nu_m M_m(t)$ can be interpreted as a step response function where $\delta(t) =$ Dirac delta function and $H(t) =$ unit step function. The purpose of introducing the integral operator is twofold. First, $\Psi_f(t) = 1$ in the time domain represents $1/\mathrm{s}$ in the Laplace frequency domain. As noted in Ref. [26], this represents the first invertible function beyond the Abel inversion based on standard mathematical tables. Second, this operation produces a parameter-free, low-pass filtering effect that assists in identifying the optimal regularization operator [26,47]. This will be clearly seen by the simulations.

B. Frequency Domain Analysis

Let us return to Eq. (4a) and let $m = 1$ for additional guidance on a good choice for $\Psi_f(t)$ [26]. Taking the Laplace transform of Eq. (4a) produces

$$\hat{\theta}(0,s) = \nu_1\sqrt{\pi}\frac{\hat{q}_s''(s)}{\sqrt{s}}, \qquad \Re(s) > 0 \tag{11a}$$

The Abel inversion [48] of Eq. (5c) leads to Eq. (4a) and can be equivalently obtained using Laplace transforms. This provides a hint on a good choice for $\Psi_f(t)$. Dividing both sides of Eq. (11a) by $\sqrt{s}$ merely leads to the Abel inversion. The next logical suggestion involves dividing Eq. (11a) by s and then inverting. Division of s in Eq. (11a) produces

$$\frac{\hat{\theta}(0,s)}{s} = \nu_1\sqrt{\pi}\frac{\hat{q}_s''(s)}{s^{3/2}}, \qquad \Re(s) > 0 \tag{11b}$$

which inverts to

$$\int_{u=0}^{t} \theta(0,u)\,\mathrm{d}u = 2\nu_1 \int_{u=0}^{t} q_s''(u)\sqrt{t-u}\,\mathrm{d}u, \qquad t \geq 0 \tag{11c}$$

since $L\{s^{-1}\} = 1$ and $L\{s^{-3/2}\} = 2\sqrt{t/\pi}$ ([46] pp. 1021–1022) and further observe that $M_1(t-u)$ is $2\sqrt{t-u}$. From this, $\Psi_f(t-u)$ is identified as unity. In the frequency domain, the transformed reduced temperature data are attenuated by a factor of $1/\mathrm{s}$.

To recap, Table 1 provides the parameters and kernels for models 1 and 2 using the conventional or natural formulation. Table 2 provides the parameters and kernels for models 1 and 2 using the preconditioned formulation when $\Psi_f(t-u) = 1$.

Table 1 Conventional approach: ν_m and $k_m(t-u)$

Model, m	ν_m	$k_m(t-u)$
$m = 1$	$\dfrac{1}{\beta\sqrt{\pi}}$	$\dfrac{1}{\sqrt{t-u}}$
$m = 2$	$\dfrac{1}{\beta\eta} = \dfrac{1}{(\rho c \Delta x)_f}$	$e^{a^2(t-u)}\operatorname{erfc}(a\sqrt{t-u})$

Table 2 Preconditioned approach: ν_m and $M_m(t-u)$

Model, m	ν_m	$M_m(t-u)$
$m=1$	$\dfrac{1}{\beta\sqrt{\pi}}$	$2\sqrt{t-u}$
$m=2$	$\dfrac{1}{\beta\eta}=\dfrac{1}{(\rho c\Delta x)_f}$	$\dfrac{\eta}{a}\left(\dfrac{2a\sqrt{t-u}}{\sqrt{\pi}}-1+e^{a^2(t-u)}\operatorname{erfc}\left(a\sqrt{t-u}\right)\right)$

IV. Future-Time Regularization and Optimal Regularization Parameter

This section offers a relatively simple and straightforward approach for estimating the source heat flux, $q_s''(t)$, from the reduced surface temperature measurement, $\theta(0,t)$. The approach taken transforms a first-kind Volterra integral equation into a second-kind integral equation (approximation possessing a regularization parameter) for the unknown source heat flux, $q_s''(t)$. This second-kind equation can produce a stable numerical approximation. This concept directly addresses system stability. For the present paper, a future-time method [21–26,49] is used for generating a second-kind Volterra equation. A family of approximations describing the source heat flux is formed based on the choice of the regularization parameter. The predictions are collected and a means for extracting the "best" prediction must be identified. In fact, this is the real crux for all inverse problems. This paper suggests developing the identification of optimal prediction using concepts from a thermal phase plane [24–26]. The first step involves a qualitative assessment, whereas the second step seeks a metric based on cross-correlation principles [24–26].

A. Regularization by a Future-Time Method

For sake of conciseness and brevity, the conventional and preconditioned formulations are concurrently regularized illustrating the existence of a uniform numerical theme. Further, each induced approximation is clearly indicated through the notational string. The future-time approach begins by advancing time through the regularization parameter now defined as $\gamma > 0$. It should be recognized that, unlike other regularization methods [19,20], causality is retained. Let $\Psi_f(t-u)=1$ and introduce future time through $t \to t+\gamma$, where γ is the future-time parameter having units of time. Doing so in each integral equation produces

$$\theta(0,t+\gamma)=\nu_m\int_{u=0}^{t+\gamma} q_s''(u)k_m(t+\gamma-u)\,\mathrm{d}u, \qquad m=1,2 \tag{12a}$$

$$\int_{u=0}^{t+\gamma}\theta(0,t+\gamma-u)\,\mathrm{d}u=\nu_m\int_{u=0}^{t+\gamma} q_s''(u)M_m(t+\gamma-u)\,\mathrm{d}u, \quad m=1,2, \qquad t\ge 0 \tag{12b}$$

respectively. At this juncture, a continuous spectrum describing γ is displayed. This will later be transformed into a discrete spectrum defined by γ_n, $n=1,2,\ldots,P$. Equations (12a) and (12b) can alternatively be expressed as

$$\theta(0,t+\gamma)=\nu_m\int_{u=0}^{t} q_s''(u)k_m(t+\gamma-u)\,\mathrm{d}u + \nu_m\int_{u=t}^{t+\gamma} q_s''(u)k_m(t+\gamma-u)\,\mathrm{d}u, \qquad m=1,2 \tag{13a}$$

$$\int_{u=0}^{t+\gamma}\theta(0,t+\gamma-u)\,\mathrm{d}u=\nu_m\int_{u=0}^{t} q_s''(u)M_m(t+\gamma-u)\,\mathrm{d}u + \nu_m\int_{u=t}^{t+\gamma} q_s''(u)M_m(t+\gamma-u)\,\mathrm{d}u, \qquad m=1,2 \tag{13b}$$

for $t\ge 0$. Formally assuming that $q_s''(u)\approx q_s''(t)$ in the small interval $u\in[t,t+\gamma]$ permits

$$\theta(0,t+\gamma)\approx\nu_m\int_{u=0}^{t} q_s''(u)k_m(t+\gamma-u)\,\mathrm{d}u + \nu_m q_s''(t)\int_{u=t}^{t+\gamma} k_m(t+\gamma-u)\,\mathrm{d}u \tag{14a}$$

$$\int_{u=0}^{t+\gamma}\theta(0,t+\gamma-u)\,\mathrm{d}u\approx\nu_m\int_{u=0}^{t} q_s''(u)M_m(t+\gamma-u)\,\mathrm{d}u + \nu_m q_s''(t)\int_{u=t}^{t+\gamma} M_m(t+\gamma-u)\,\mathrm{d}u, \quad m=1,2, \qquad t\ge 0 \tag{14b}$$

Simplifying and recovering the equal sign requires

$$\theta(0,t+\gamma)=\nu_m\int_{u=0}^{t} q_{s,\gamma}''(u)k_m(t+\gamma-u)\,\mathrm{d}u+\nu_m C_\gamma^m q_{s,\gamma}''(t) \tag{15a}$$

$$\int_{u=0}^{t+\gamma}\theta(0,t+\gamma-u)\,\mathrm{d}u=\nu_m\int_{u=0}^{t} q_{s,\gamma}''(u)M_m(t+\gamma-u)\,\mathrm{d}u + \nu_m D_\gamma^m q_{s,\gamma}''(t), \qquad t\ge 0 \tag{15b}$$

where $q_{s,\gamma}''(t)\approx q_s''(t)$ and

$$C_\gamma^m=\int_{u=t}^{t+\gamma}k_m(t+\gamma-u)\,\mathrm{d}u=\int_{z=0}^{\gamma}k_m(z)\,\mathrm{d}z \tag{15c}$$

$$D_\gamma^m=\int_{u=t}^{t+\gamma}M_m(t+\gamma-u)\,\mathrm{d}u=\int_{z=0}^{\gamma}M_m(z)\,\mathrm{d}z \tag{15d}$$

Equations (15a) and (15b) are now Volterra integral equations of the second kind [42] for $q_{s,\gamma}''(t)$. Good stability characteristics should prevail for sufficiently large $\nu_m C_\gamma^m$ and $\nu_m D_\gamma^m$. A very small value of γ retains too many high frequencies in the signal, thereby leading to an unstable prediction of source heat flux. In contrast, an excessively large value of γ does not retain enough high frequencies in the signal, thus leading to oversmoothing in the predicted source heat flux.

To implement this regularization approach, departure from the continuous time variable, t, is required. The discrete sampling times are defined as t_i, $i=1,2,\ldots,N$, where N represents the number of data points beyond the initial condition. Here, $t_i=i\Delta t$ such that $\Delta t=t_{\max}/\mathrm{N}$. Data collection terminates at $t=t_{\max}$. A corresponding discrete spectrum of future-time parameters are now needed and expressed as γ_n, $n=1,2,\ldots,P$. It is convenient to define γ_n in terms of the sampling step. This leads to $\gamma_n=nM_f\Delta t$, $n=1,2,\ldots,P$, where M_f is a convenient multiplication factor.

The discrete forms for Eqs. (15a) and (15c) and Eqs. (15b) and (15d) are given as

$$\theta(0,t_i+\gamma_n)=\nu_m\int_{u=0}^{t_i} q_{s,\gamma_n}''(u)k_m(t_i+\gamma_n-u)\,\mathrm{d}u + \nu_m C_{\gamma_n}^m q_{s,\gamma_n}''(t_i) \tag{16a}$$

$$\int_{u=0}^{t_i+\gamma_n}\theta(0,t_i+\gamma_n-u)\,\mathrm{d}u=\nu_m\int_{u=0}^{t_i} q_{s,\gamma_n}''(u)M_m(t_i+\gamma_n-u)\,\mathrm{d}u + \nu_m D_{\gamma_n}^m q_{s,\gamma_n}''(t_i), \quad i=1,2,\ldots,N-nM_f, \qquad n=1,2,\ldots,P \tag{16b}$$

respectively, where

$$C_{\gamma_n}^m=\int_{z=0}^{\gamma_n}k_m(z)\,\mathrm{d}z, \qquad m=1,2, \qquad n=1,2,\ldots,P \tag{16c}$$

$$D_{\gamma_n}^m=\int_{z=0}^{\gamma_n}M_m(z)\,\mathrm{d}z, \qquad m=1,2, \qquad n=1,2,\ldots,P \tag{16d}$$

Observe that the resolvable or effective time domain is decreased from $t_{\max}$ to $t_{\max} - nM_f\Delta t, n = 1, 2, \ldots, P$. A consistent numerical integration method is used based on a product trapezoial rule [42]. The notational flow or explicit chain of events in the approximation is important in analysis. With this said, discretizing Eq. (16) leads to $q_s''(t) \approx q_{s,\gamma}''(t) = q_{s,\gamma_n}''(t) \approx q_{s,\gamma_n,N}''(t)$. Incorporating noisy data into the equations leads to the final notation $q_s''(t) \approx q_{s,\gamma}''(t) = q_{s,\gamma_n}''(t) \approx q_{s,\gamma_n,N}''(t) \approx \tilde{q}_{s,\gamma_n,N}(t)$.

B. Thermal Phase Plane and Cross Correlation for Estimating γ_{opt}

It is enlightening to review stability using both qualitative and quantitative means. This is especially important for understanding the connection between physics and mathematics. The heat equation possesses a time derivative of the temperature [Eq. (2a)] or heat flux [Eq. (3d)]. All reconstructions are propagated through the fundamental field equation that inherently contains certain continuity expectations. With this said, a logical parameterized plot involving the thermal phase plane seems highly reasonable. This could allow for a quick and simple qualitative view of stability as it is well known that the time derivative of experimental data is highly unstable [50,51]. Instability increases as the sampling rate increases (due to intrinsic time differentiation of data). The thermal phase plane, for this study, is defined by a plot of $(\mathrm{d}q_s''/\mathrm{d}t)(t)$ against $q_s''(t)$.

Conventional mathematical convergences do not exist for ill-posed problems. However, an alternative point of view, in terms of patterns and pattern development, seems appropriate for this framework. With that said, cross correlation [24–26] seems to provide a means for comparing predictive paired sequences. If a normed source heat flux error over the regularization parameter is available, then a minimum would be observed defining the optimal regularization parameter. Clearly, in an experimental setting this does not exist.

Let the source heat flux cross-correlation coefficient be given as [24–26]

$$R_q(\tilde{q}_{s,\gamma_n,N}'', \tilde{q}_{s,\gamma_{n+1},N}'') = \frac{\sum_{j=0}^{N-(n+1)M_f} \tilde{q}_{s,\gamma_n,N}''(0,t_j)\tilde{q}_{s,\gamma_{n+1},N}''(0,t_j)}{\sqrt{\sum_{j=0}^{N-(n+1)M_f} (\tilde{q}_{s,\gamma_n,N}''(0,t_j))^2 \sum_{j=0}^{N-(n+1)M_f} (\tilde{q}_{s,\gamma_{n+1},N}''(0,t_j))^2}} \tag{17a}$$

$n = 1, 2, \ldots, P-1$, while the source heat flux rate cross-correlation coefficient be given as [25,26]

$$R_{\dot{q}}(\dot{\tilde{q}}_{s,\gamma_n,N}'', \dot{\tilde{q}}_{s,\gamma_{n+1},N}'') = \frac{\sum_{j=0}^{N-(n+1)M_f} \dot{\tilde{q}}_{s,\gamma_n,N}''(0,t_j)\dot{\tilde{q}}_{s,\gamma_{n+1},N}''(0,t_j)}{\sqrt{\sum_{j=0}^{N-(n+1)M_f} (\dot{\tilde{q}}_{s,\gamma_n,N}''(0,t_j))^2 \sum_{j=0}^{N-(n+1)M_f} (\dot{\tilde{q}}_{s,\gamma_{n+1},N}''(0,t_j))^2}} \tag{17b}$$

$n = 1, 2, \ldots, P-1$. Phase shift is not included in this analysis [24]. The interested reader should consult Ref. [24] for an alternative methodology for estimating the regularization parameter based on phase shift and its general behavior as the future-time parameter is increased. Further, as indicated in Ref. [47], both attenuation and delay effects can be visually seen when an oscillatory heat flux input is imposed and models are compared.

It will be evident [5] that driving $R_q(\tilde{q}_{s,\gamma_n,N}'', \tilde{q}_{s,\gamma_{n+1},N}'')$ to unity is easily accomplished. However, smoothness is controlled by the source heat flux rate as previously noted. Interpreting the rate term, $R_{\dot{q}}(\dot{\tilde{q}}_{s,\gamma_n,N}'', \dot{\tilde{q}}_{s,\gamma_{n+1},N}'')$, is fundamental for defining the optimal future-time parameter. Oversmoothing is approached as $R_{\dot{q}}(\dot{\tilde{q}}_{s,\gamma_n,N}'', \dot{\tilde{q}}_{s,\gamma_{n+1},N}'') \to 1$. This limiting case attempts to extract more accuracy out of the data than possible. To reiterate, cross correlation is used to describe the alignment or the formation of a pattern. The thermal phase plane plot assists to qualitatively display the onset of a pattern. The onset of the pattern leads to the optimal regularization parameter, γ_{opt}. This has been demonstrated in Refs. [24–26].

Table 3 Simulation parameters

Parameter/property	Value	Unit
c (Macor)	790	$\mathrm{J/(kg \cdot K)}$
c (platinum)	130	$\mathrm{J/(kg \cdot K)}$
Δx	0.5	μm
Δt	1.0	μs
ϵ_T (noise factor)	0.03	— —
k (Macor)	1.46	$\mathrm{W/(m \cdot K)}$
M_f	3	— —
N (data)	100	— —
ρ (Macor)	2,531	$\mathrm{kg/m^3}$
ρ (platinum)	21,400	$\mathrm{kg/m^3}$
$q_{\max}''$	300	$\mathrm{W/cm^2}$
$t_{\max}$	0.0001	s

V. Results

This section provides preliminary numerical clarity and results illustrating the benefits of the proposed preconditioned data reduction equation for the two proposed models in the recovery of the source heat flux, $q_s''(t)$. For this study, the thin film is composed of pure platinum,[‡] which is ideally adhered to the Macor[§] substrate per Fig. 1. The source heat flux, to be studied in this paper, is given as ([40] Fig. 5)

$$q_s''(t) = q_{\max}'', \qquad t \in [0, t_{\max}] \tag{18}$$

for practical shock tunnel applications. The interested reader can review Ref. [47] for a highly transient heat flux given as

$$q_s''(t) = q_{\max}''(e^{-((t-\tau_1)/\sigma_1)^2} + 0.75e^{-((t-\tau_2)/\sigma_2)^2}), \qquad t \geq 0$$

The reduced temperature data are produced using

$$\theta_i = \theta(0,t_i) + \epsilon_T\|\theta(0,t)\|_\infty r_i, \qquad i = 1, 2, \ldots, N \tag{19}$$

where $\theta(0,t)$ is the exact (or numerically "exact") model-based reduced surface temperature obtained by solving the direct or forward problem. Here, the infinity norm is defined as $\|h\|_\infty = \max_{t\in[0,t_{\max}]}|h|$, while r_i, $i = 1, 2, \ldots, N$, denotes the ith drawn random number from the interval $[-1, 1]$. Table 3 provides the parameters for the simulations. Figure 2 displays the source heat flux described by Eq. (18) using the parameters defined in Table 3.

As this study is numerical in nature, the generated surface temperature data for fixed source heat flux varies with the chosen model. In practice, only a single set of surface temperature data exists.

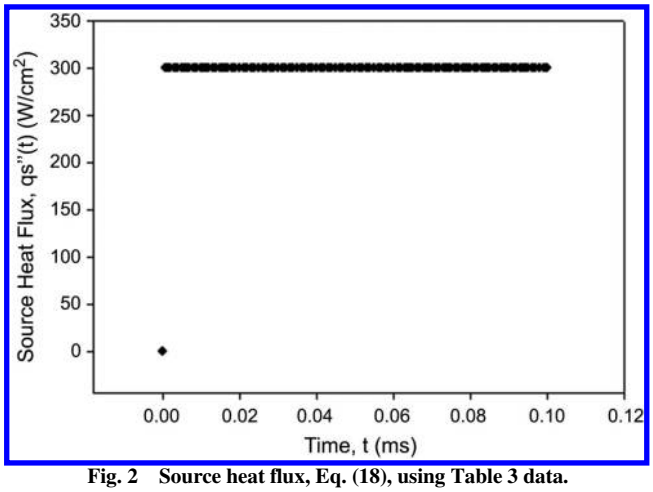

Fig. 2 Source heat flux, Eq. (18), using Table 3 data.

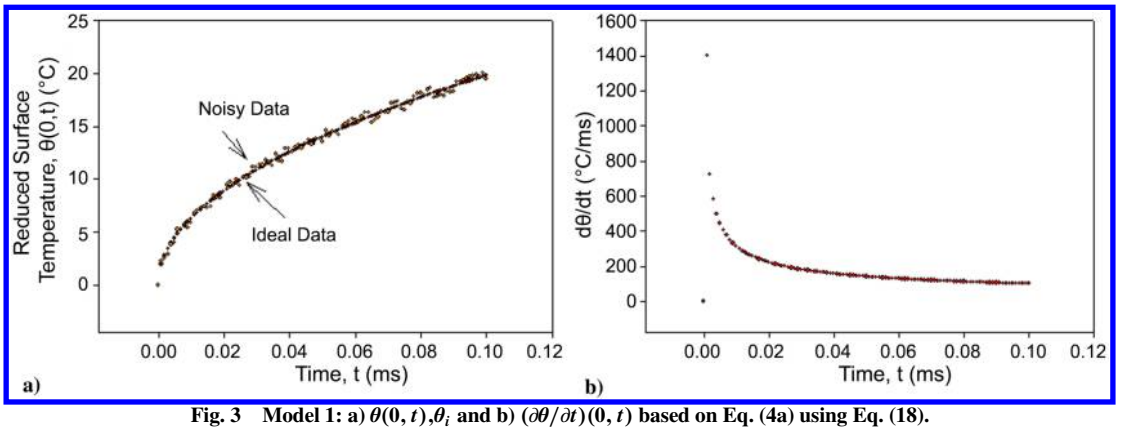

Fig. 3 Model 1: a) $\theta(0,t)$,θ_i and b) $(\partial\theta/\partial t)(0,t)$ based on Eq. (4a) using Eq. (18).

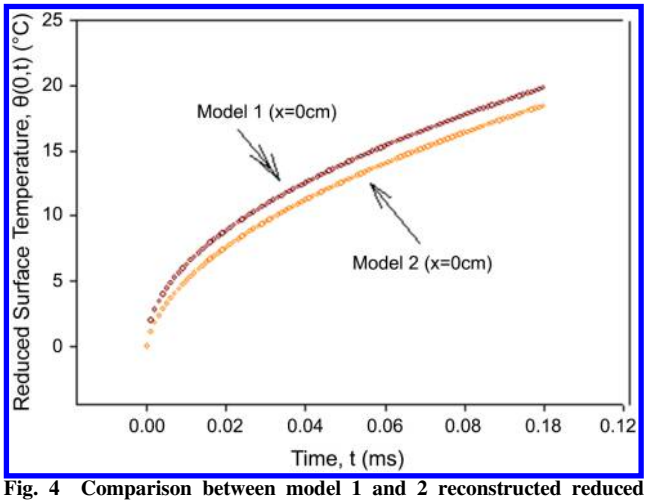

Fig. 4 Comparison between model 1 and 2 reconstructed reduced surface temperatures.

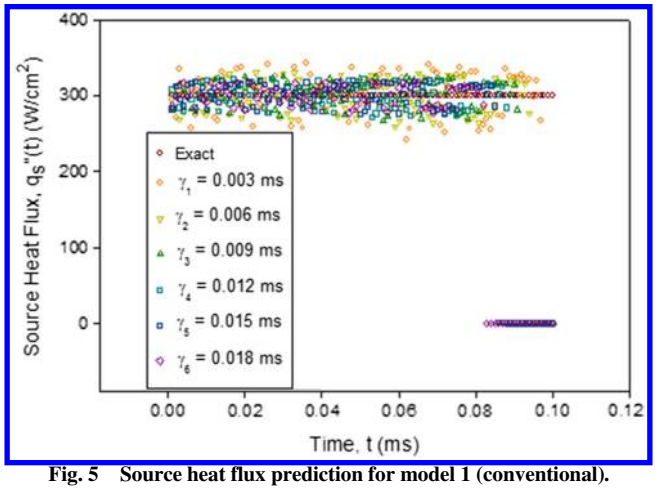

Fig. 5 Source heat flux prediction for model 1 (conventional).

Thus, this study focuses on the formulation and implementation of the regularization method for resolving each model equation; that is, for fixed model (1 or 2) temperature data are constructed per the exact solution of the model. The imposed preconditioned approach can be compared with the conventional approach for fixed model. If experimental data are available, then a single set of reduced temperature data can be used. For brevity, noiseless data results are not presented (though studied) as it validates the numerical method.

A. Model 1: Conventional and Preconditioned Predictions

Before delving into the results, it appears germane to provide some graphical *indications* describing both surface temperature and time rate of change of the surface temperature. Model 1 can be used for this insight. It is important to note that most studies do not actually provide the *heating rate* as defined by $(\partial T/\partial t)(0,t)$. This quantity is actually important to present [see Eq. (6e)].

Table 3 parameters are reflective of the parameters used and results obtained by Flaherty and Austin ([40] Fig. 5). In fact, the heating rate appears to be as high as 150,000 K/s (or more) [40]. With this said, Figs. 3a and 3b provide the Macor reduced surface temperature (°C) via Eq. (4a) and heating rate (°C/s) as calculated by a low-order finite difference method. For model 1 $\Delta x = 0$ and using the parameters described in Table 3, the heating rate shown in Fig. 3b is significant. It is important to visualize the difference between the reconstructed reduced surface temperature using the identical heat flux source given by Eq. (18). Figure 4 displays the reduced surface temperature histories for both model 1 and model 2. Measured temperatures relate the true physics that accounts for the energy balance, property variations, and dimensionality, and may need to be adjusted to account for the sensor intrusiveness. The most inclusive model should approach the measured temperatures for a given heat flux. Hence, simulated model 2 temperatures used in model 1 can incorrectly predict the surface heat flux.

Focus is presently directed to model 1 using the conventional analytic formulation described by Eq. (4a). Figures 5–7 describe the reconstructed source heat flux as a function of the regularization parameter, γ_n; resulting thermal phase diagram as a function of

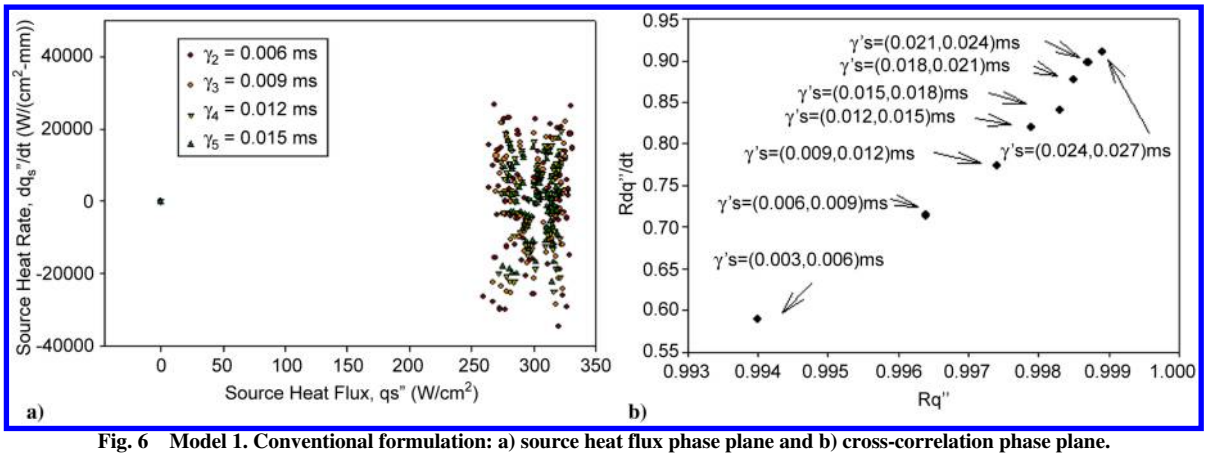

Fig. 6 Model 1. Conventional formulation: a) source heat flux phase plane and b) cross-correlation phase plane.

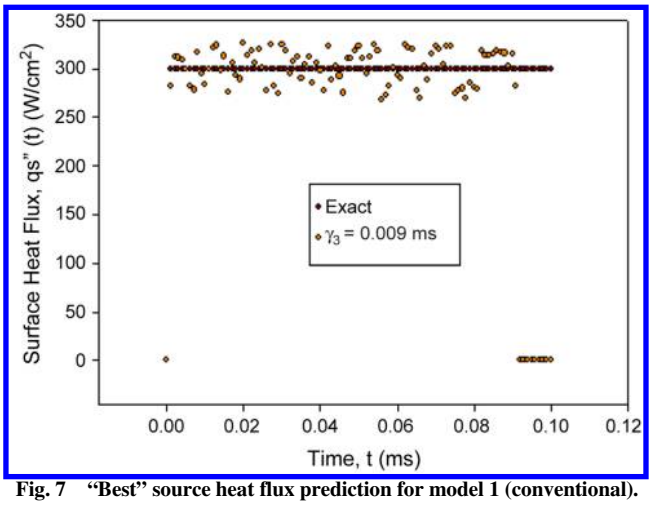

Fig. 7 "Best" source heat flux prediction for model 1 (conventional).

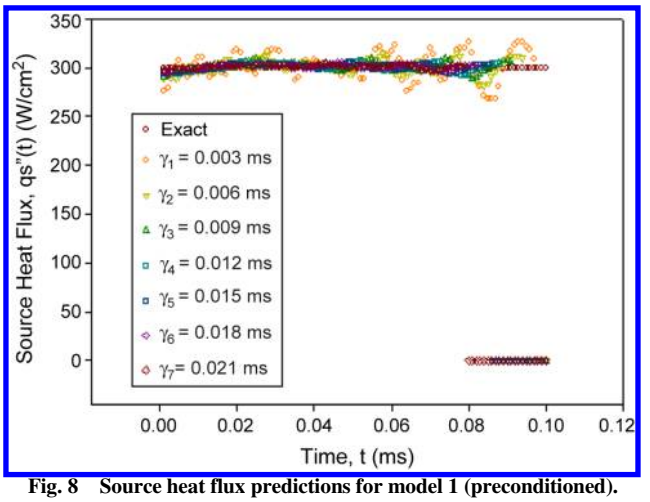

Fig. 8 Source heat flux predictions for model 1 (preconditioned).

several regularization parameters; and cross-correlation phase diagram. Figure 5 displays the reconstructed source heat flux using model 1 and the conventional numerical method for the indicated values of regularization parameter, γ_n, $n = 1, \ldots, 6$. The exact heat flux is shown in this figure as a basis for comparison. It is observed that, as γ_n increases, beyond some optimal condition, additional smoothing occurs and that it is difficult to discern a favorable comparison with the exact function, Eq. (18).

Figure 6a presents the previously described thermal phase plane. It is difficult to discern the onset of a pattern and apparently renders the phase-plane concept for extracting the regularization parameter meaningless. Figure 6b presents the corresponding cross-correlation phase plane for pairings (γ_n, γ_{n+1}), $n = 1, 2, \ldots, 8$. Here, the cross-correlation coefficient for the source heat flux, $R_q(\tilde{q}''_{s,\gamma_n,N}, \tilde{q}''_{s,\gamma_{n+1},N})$, moves toward the value of unity (as desired). The cross-correlation coefficient source heat flux rate $R_{\dot{q}}(\tilde{q}''_{s,\gamma_n,N}, \tilde{q}''_{s,\gamma_{n+1},N})$ propagates to unity in a near linear fashion. It should be noted that if a Gauss heat flux [47] is imposed, then insufficient movement toward unity is noted for the cross-correlation coefficient for the heat flux rate, and thus renders difficulties in identifying the optimal regularization parameter. The constant heat flux case is a relatively easy function to reconstruct.

Figures 8–10 correspond to the previous sequence of plots associated with the conventional integral formulation; however, this series of results are associated with the preconditioned method where $\Psi_f(t-u) = 1$. The identical data set and numerical integration rules are implemented. In stark contrast, a different story is now conveyed. Figure 8 mimics the choice of regularization parameters of Fig. 5. However, in this case, the preconditioned approach renders results possessing significantly less error than the conventional integral formulation.

Figure 9a presents the thermal phase plane that clearly indicates the onset of a pattern as γ_n is varied. Figure 9b presents the cross-correlation phase plane where, unlike Fig. 6b, the points congregate at unity. Care must be taken as results too close to unity for $R_{\dot{q}}(\tilde{q}''_{s,\gamma_n,N}, \tilde{q}''_{s,\gamma_{n+1},N})$ violate physical expectations as noise exists in the data. As with filtering, some blending of science and art is required to interpret results. An imaginary vertical asymptote provides guidance for choosing the optimal regularization set. It is always best to retain as much high frequency in the signal as possible. Figure 10 presents the exact source heat flux and predictions based on

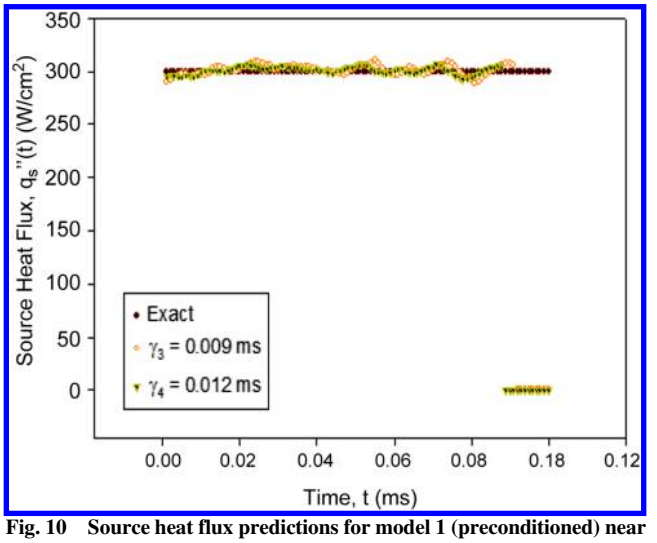

Fig. 10 Source heat flux predictions for model 1 (preconditioned) near optimal conditions.

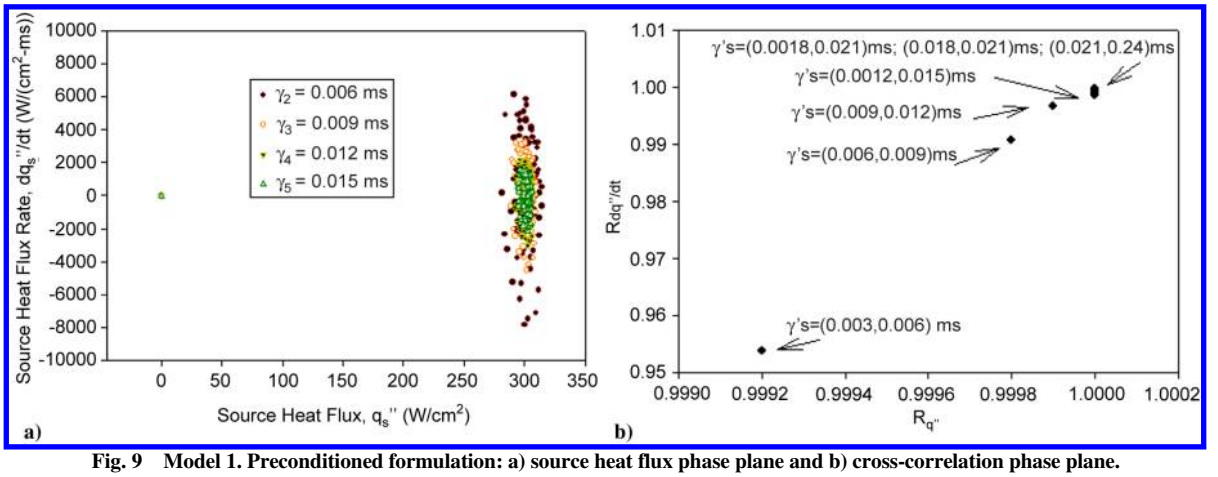

Fig. 9 Model 1. Preconditioned formulation: a) source heat flux phase plane and b) cross-correlation phase plane.

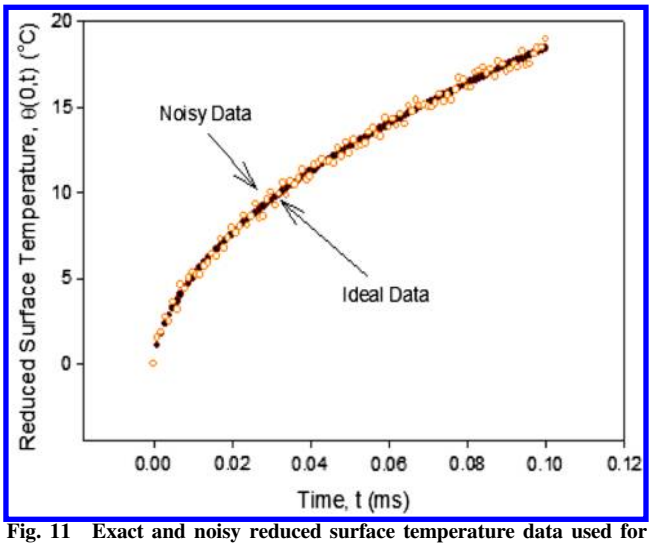

Fig. 11 Exact and noisy reduced surface temperature data used for model 2.

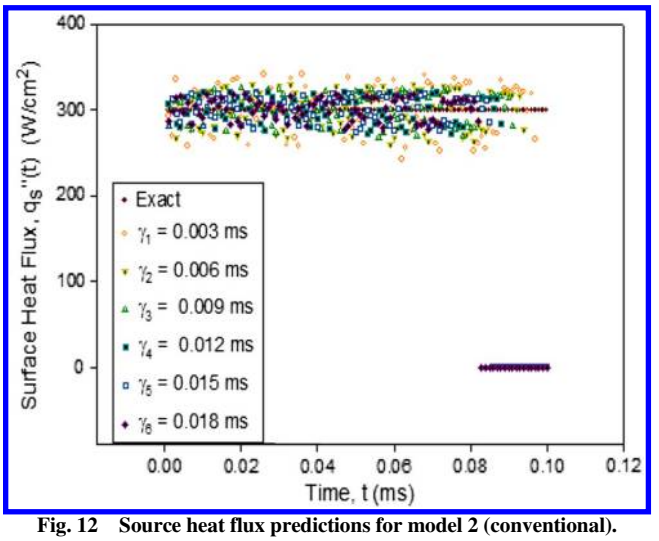

Fig. 12 Source heat flux predictions for model 2 (conventional).

γ_3 and γ_4. Both results are excellent in the context of this numerical experiment. The source heat flux prediction using γ_3 contains more high-frequency content in the signal than the results from γ_4. In general, preserving higher frequencies in the signal is often better than seeking a "smooth" result especially when a time-varying heat source is present. Therefore, for model 1, the new preconditioned approach produces superior predictions. Maybe more important, it is possible to characterize the "optimal" regularization parameter leading to the "best" prediction.

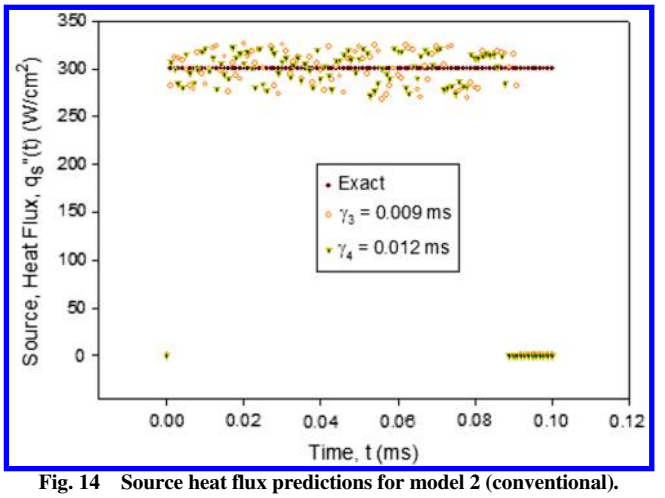

Fig. 14 Source heat flux predictions for model 2 (conventional).

B. Model 2: Conventional and Preconditioned Predictions

Following a similar presentation path as outlined in the discussion of the results for model 1, Fig. 11 presents the noisy reduced surface temperature data used in the following simulations. Figure 12 displays the family of source heat flux predictions using various regularization parameters, γ_n, $n = 1, 2, \ldots, 6$, based on the conventional integral formulation. Again, the conventional formulation produces relatively large oscillations in the projection.

Figure 13 presents the thermal phase plane and cross-correlation phase plane. Similar characteristics are observed with that of the model 1 (conventional formulation) examination. Figure 14 displays the optimal prediction illustrating the "best" extractable prediction for this set of regularization parameters.

The last set of figures further endorses the utility of the proposed preconditioner. This is demonstrated through model 2, which possesses additional sophistication and detail over model 1. Figures 15–17 correspond to the previous sequence of plots associated with the conventional integral formulation; however, this series of results are associated with the preconditioned method where $\Psi_f(t-u) = 1$. The identical data set and numerical integration rules are implemented (model 2). Figure 15 presents the family of source heat flux predictions developed from the indicated discrete spectrum of regularization parameters. Figure 15 mimics the choice of regularization parameters displayed in Fig. 12. In this case, the preconditioned ("parameter-free") approach renders results possessing significantly less error than the conventional integral formulation. Figure 16a presents the thermal phase plane that clearly indicates the onset of a pattern as γ_n is varied. Again, only a small set (for clarity) of phase plane results are indicated though qualitatively one could argue that the jump from instability to stability occurs near γ_3 [24–26]. Figure 16b presents the cross-correlation phase plane displaying that a clear and progressive approach to unity is occurring for both $R_q(\tilde{q}''_{s,\gamma_n,N}, \tilde{q}''_{s,\gamma_{n+1},N})$ and $R_{\dot{q}}(\dot{\tilde{q}}''_{s,\gamma_n,N}, \dot{\tilde{q}}''_{s,\gamma_{n+1},N})$. Following our

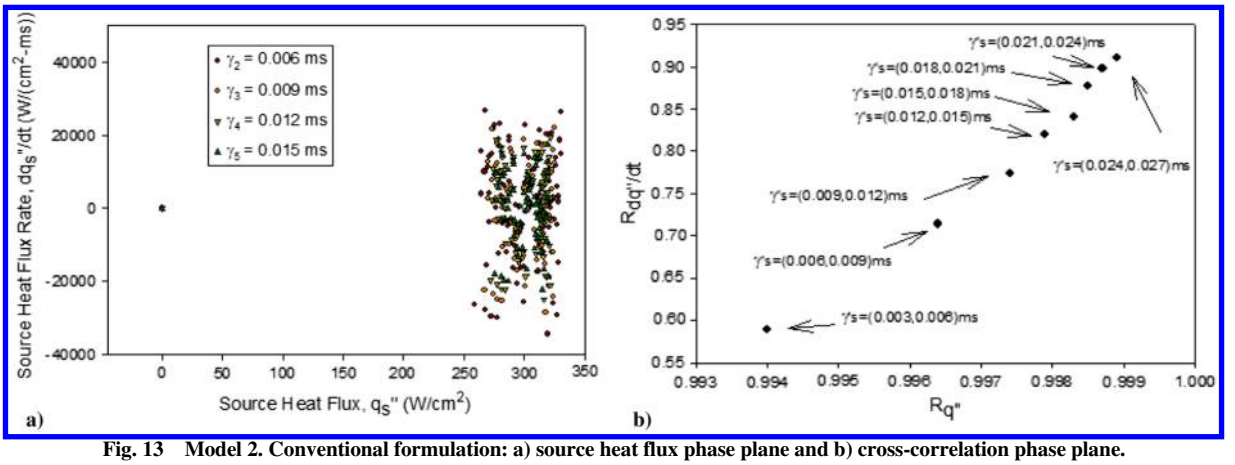

Fig. 13 Model 2. Conventional formulation: a) source heat flux phase plane and b) cross-correlation phase plane.

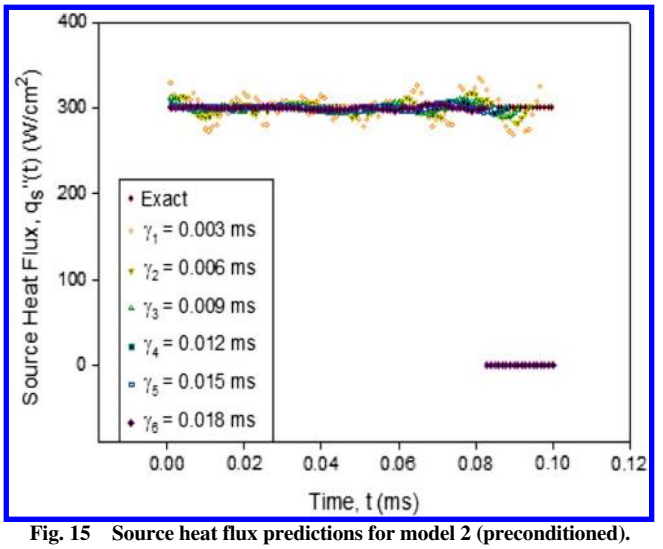

Fig. 15 Source heat flux predictions for model 2 (preconditioned).

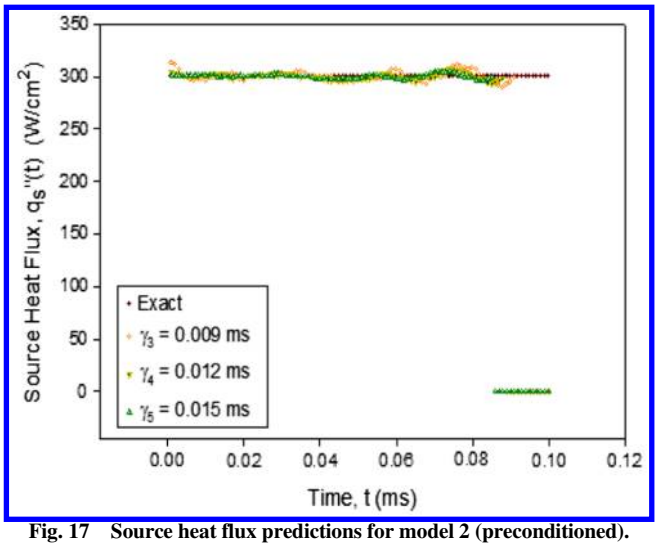

Fig. 17 Source heat flux predictions for model 2 (preconditioned).

previous discussions, we can identify candidate optimal parameters of γ_n. From Fig. 16b, γ_3 to γ_5 are suggested.

Figure 17 presents the exact source heat flux and predictions based on γ_3 to γ_5. Results are excellent in the context of this numerical experiment. The predicted source heat flux, using γ_3, contains more high-frequency content in the signal than the results from γ_4. Therefore, for model 2, the new preconditioned approach produces superior predictions. More important, it is possible to characterize the "optimal" regularization parameter leading to the "best" prediction.

VI. Conclusions

A thorough analytical study has been undertaken illustrating the importance of modeling and analysis for investigating and understanding data reduction relationships associated with thin-film temperature sensors for recovering the source heat flux. The extended modeling effort provides additional assurance in the reconstruction process when highly rapid transients are occurring (i.e., when $(\rho c\Delta x)_f(\partial\theta/\partial t)(0,t))$ is not relatively small when compared with $q_s''(t)$). In this case, the inclusion of the storage of energy in the model of the thin-film/substrate system should be accounted. In fact, model 2 is closer to reality. Hence, using the measured temperatures and model 1 will lead to an underestimation of the heat flux for the example displayed in this paper. Finally, the preconditioned solution based on the concept of a step response function produces accurate predictions whereby the optimal regularization parameter can be identified using thermal phase plane concepts. To reiterate, the preconditioned formulation offers several attributes. First, the predictions are noticeably more accurate than the conventional formulation. Second, extracting the optimal regularization parameter by the thermal phase concept now becomes available. Third, the extended model should be considered as it does not cause any mathematical difficulties. It should be recalled that uncertainty analysis [52] depends on the chosen model. Hence, "missing physics" can contribute to a misunderstanding of the uncertainty propagation.

Appendix : Limiting Process in Models

It is important to demonstrate that Eq. (7b) reduces to Eq. (4a) as $\Delta x \to 0$ (or similarly $(\rho c\Delta x)_f \to 0)$). Let us explicitly express Eq. (7b) as

$$\theta(0,t) = \frac{1}{(\rho c\Delta x)_f}\int_{u=0}^{t} q_s''(u)e^{\beta^2(t-u)/(\rho c\Delta x)_f^2} \times \operatorname{erfc}\left(\frac{\beta}{(\rho c\Delta x)_f}\sqrt{t-u}\right)\mathrm{d}u, \qquad t \geq 0 \tag{A1}$$

Next, let $z = (\beta\sqrt{t-u}/(\rho c\Delta x)_f) \geq 0$. As $\Delta x \to 0$ for $t-u>0$ then $z \to \infty$. The asymptotic analysis of the integrand is performed before integration. The complementary error function can be expressed in terms of its integral definition as ([46] p. 297)

$$\operatorname{erfc}(z) = \frac{2}{\sqrt{\pi}}\int_{u=z}^{\infty} e^{-u^2}\,\mathrm{d}u = \frac{2}{\sqrt{\pi}}\int_{u=z}^{\infty}\left(\frac{-1}{2u}\right)\frac{d}{du}e^{-u^2}\,\mathrm{d}u, \qquad z \geq 0 \tag{A2}$$

or upon integration by parts leads to

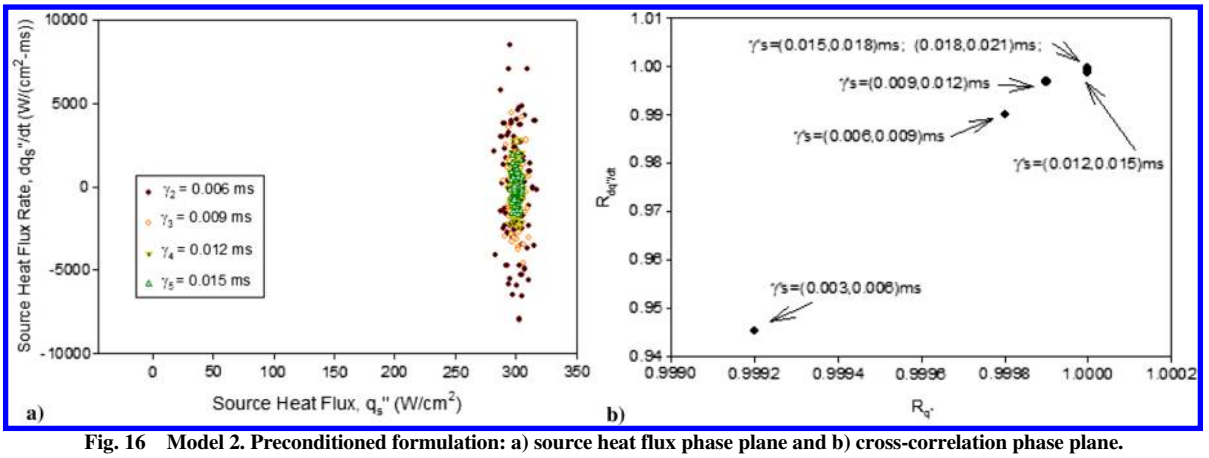

Fig. 16 Model 2. Preconditioned formulation: a) source heat flux phase plane and b) cross-correlation phase plane.

$$\operatorname{erfc}(z) = \frac{2}{\sqrt{\pi}}\left(-\frac{1}{2u}e^{-u^2}|_{u=z}^{\infty} - \int_{u=z}^{\infty}\frac{1}{2u^2}e^{-u^2}\,\mathrm{d}u\right)$$
$$= \frac{2}{\sqrt{\pi}}\left(-\frac{1}{2u}e^{-u^2}|_{u=z}^{\infty} + \int_{u=z}^{\infty}\frac{1}{4u^3}\frac{d}{du}e^{-u^2}\,\mathrm{d}u\right)$$

Performing this procedure a second time yields

$$\operatorname{erfc}(z) = \frac{2}{\sqrt{\pi}}\left(-\frac{1}{2u}e^{-u^2}|_{u=z}^{\infty} + \frac{e^{-u^2}}{4u^3}\Big|_{u=z}^{\infty} + \int_{u=z}^{\infty}\frac{3}{4u^4}e^{-u^2}\,\mathrm{d}u\right)$$

The pattern is now readily established. It can be shown that the leading order behavior produces

$$\operatorname{erfc}(z) = \frac{2}{\sqrt{\pi}}\left(\frac{1}{2z}e^{-z^2} - \frac{1}{4z^3}e^{-z^2} + \ldots\right) \tag{A3}$$

or in asymptotic notation

$$\operatorname{erfc}(z) \sim \frac{2}{\sqrt{\pi}}\left(\frac{1}{2z}e^{-z^2} - \frac{1}{4z^3}e^{-z^2}\right), \qquad \text{as } z \to \infty$$

Substituting Eq. (A3) into Eq. (A1) renders

$$\theta(0,t) = \frac{2}{\sqrt{\pi}}\frac{1}{(\rho c\Delta x)_f}\int_{u=0}^{t} q_s''(u)e^{(\beta\sqrt{t-u}/(\rho c\Delta x)_f)^2}e^{-(\beta\sqrt{t-u}/(\rho c\Delta x)_f)^2}$$
$$\left(\frac{1}{2(\beta\sqrt{t-u}/(\rho c\Delta x)_f)} - \frac{1}{4(\beta\sqrt{t-u}/(\rho c\Delta x)_f)^3} + \ldots\right)\mathrm{d}u,$$
$$t \geq 0$$

Taking the limit as $\Delta x \to 0$ (or $z \to \infty$) produces

$$\lim_{\Delta x\to 0}\theta(0,t) = \lim_{\Delta x\to 0}\frac{2}{\sqrt{\pi}}\int_{u=0}^{t} q_s''(u)$$
$$\times\left(\frac{1}{2\beta\sqrt{t-u}} - \frac{(\rho c\Delta x)_f^2}{4(\beta\sqrt{t-u})^3} + \ldots\right)\mathrm{d}u$$

or

$$\theta(0,t) = \frac{2}{\sqrt{\pi}}\int_{u=0}^{t} q_s''(u)\lim_{\Delta x\to 0}\left(\frac{1}{2\beta\sqrt{t-u}} - \frac{(\rho c\Delta x)_f^2}{4(\beta\sqrt{t-u})^3} + \ldots\right)\mathrm{d}u$$

thereby

$$\theta(0,t) = \frac{1}{\beta\sqrt{\pi}}\int_{u=0}^{t}\frac{q_s''(u)}{\sqrt{t-u}}\,\mathrm{d}u, \qquad t \geq 0$$

which replicates Eq. (4a).

Acknowledgment

The work developed here was supported by a grant provided by the National Science Foundation (NSF-CBET-1703442).

References

[1] Diller, T. E., "Advances in Heat Flux Measurements," *Advances in Heat Transfer*, Vol. 23, Academic Press, New York, 1993, pp. 279–368.

[2] Gulhan, A., "Heat Flux Measurements in High Enthalpy Flows," Defense Technical Information Center ADP010750, April 2000, pp. 1–18.

[3] Chazot, O., "Experimental Studies on Hypersonic Stagnation Point Chemical Environment," NATO RTO-EN-AVT-142, 2007, pp. 13-1–13-32.

[4] Schultz, D. L., and Jones, T. V., "Heat Transfer Measurements in Short-Duration Hypersonics Facilities," NATO AGARD-AG-165, 1973. pp. 1–55.

[5] Marineau, E. C., and Hornung, H., "Modeling and Calibration of Fast-Response Coaxial Heat Flux Gages," *47th AIAA Aerospace Sciences Meeting*, AIAA Paper 2009-737, Jan. 2009.

[6] Coblish, J. J., Coulter, S. M., and Norris, J. D., "Aerothermal Measurement Improvements Using Coaxial Thermocouples at AEDC Hypervelocity Wind Tunnel No. 9," *45th AIAA Aerospace Sciences Meeting*, AIAA Paper 2007-1467, Jan. 2007.

[7] Desikan, S. L. N., Suresh, K., Srinivasan, K., and Raveendran, P. G., "Fast Response Co-Axial Thermocouple for Short Duration Impulse Facilities," *Applied Thermal Engineering*, Vol. 96, March 2016, pp. 48–56. doi:10.1016/j.applthermaleng.2015.11.074

[8] Menezes, V., and Bhat, S., "A Coaxial Thermocouple for Shock Tunnel Applications," *Review of Scientific Instrumentation*, Vol. 81, No. 10, 2010, Paper 104905. doi:10.1063/1.3494605

[9] Li, J., Chen, H., Zhang, S., Zhang, X., and Yu, H., "On the Response of Coaxial Surface Thermocouples for Transient Aerodynamic Heating Measurements," *Experimental Thermal and Fluid Science*, Vol. 86, Sept. 2017, pp. 141–148. doi:10.1016/j.expthermflusci.2017.04.011

[10] Hollis, B. R., Thompson, R. A., Berry, S. A., Horvath, T. J., Murphy, K. J., Nowak, R. J., and Alter, S. J., "X-33 Computational Aeroheating/ Aerodynamic Predictions and Comparisons with Experimental Data," NASA TP-2003-212600, May 2003.

[11] Liu, T., Campbell, B. T., Sullivan, J. P., Lafferty, J., and Yanta, W., "Heat Transfer Measurement on a Waverider at Mach 10 Using Fluorescent Paint," *Journal of Thermophysics and Heat Transfer*, Vol. 9, No. 4, 1995, pp. 605–611. doi:10.2514/3.714

[12] Schramm, J. M., Hannemann, K., Ozawa, H., Beck, W., and Klein, C., "Development of Temperature Sensitive Paints for the High Enthalpy Shock Tunnel Gottinggen, HEG," *Proceedings of the 8th European Symposium on Aerothermodynamics for Space Vehicles*, Lisbon, Portugal, March 2015.

[13] Yang, L., Zare-Behtash, H., Erdem, E., and Kontis, K., "Investigation of the Double Ramp in Hypersonic Flow Using Luminescent Measurement System," *Experimental Thermal and Fluid Science*, Vol. 40, July 2012, pp. 50–56. doi:10.1016/j.expthermflusci.2012.01.032

[14] Kurtis, I., and Lewis, M. J., "Global Temperature Sensitive Paint System for Heat Transfer Measurements in Long-Duration Hypersonic Flows," *Journal of Thermophysics and Heat Transfer*, Vol. 23, No. 2, 2009, pp. 256–266. doi:10.2514/1.39926

[15] Liu, T., Cai, Z., Lai, J., Rubal, J., and Sullivan, J. P., "Analytical Method for Determining Heat Flux from Temperature-Sensitive-Paint Measurements in Hypersonic Tunnels," *Journal of Thermophysics and Heat Transfer*, Vol. 24, No 1, 2010, pp. 85–94. doi:10.2514/1.43372

[16] Liu, T., Ward, C. A. C., Rubal, J., Sullivan, J. P., and Schneider, S. P., "Heat-Flux Measurements with Temperature Sensitive Paint in a Mach-6 Quiet Tunnel," *Journal of Spacecraft and Rockets*, Vol. 50, No. 2, 2013, pp. 282–293. doi:10.2514/1.A32311

[17] Cai, Z., Liu, T., Wang, B., Rubal, J., and Sullivan, J. P., "Numerical Inverse Heat Transfer Analysis for Temperature-Sensitive-Paint Measurements in Hypersonic Tunnels," *Journal of Thermophysics and Heat Transfer*, Vol. 25, No. 1, 2011, pp. 59–67. doi:10.2514/1.49217

[18] Kurits, I., Norris, J. D., and Bhandari, P., "Temperature-Sensitive Paint Calibration Methodology Developed at AEDC Tunnel 9," *49th AIAA Aerospace Sciences Meeting*, AIAA Paper 2011-851, Jan. 2011.

[19] Kurpisz, K., and Nowak, A. J., *Inverse Thermal Problems*, Computational Mechanics Publ., Southampton, U.K., 1995, pp. 1–34.

[20] Beck, J. V., Blackwell, B., and St. Clair, C. R., Jr., *Inverse Heat Conduction*, Wiley, New York, 1985, pp. 1–50.

[21] Frankel, J. I., Keyhani, M., and Elkins, B. E., "Surface Heat Flux Prediction through Physics-Based Calibration—Part 1: Theory," *AIAA Journal of Thermophysics and Heat Transfer*, Vol. 27, No. 2, 2013,

[‡]Data available online at http://periodictable.com/Elements/078/data.html [retrieved 20 September 2018].

[§]Data available online at https://www.corning.com/media/worldwide/csm/documents/71759a443535431395eb34ebead091cb.pdf [retrieved 30 September 2018].

pp. 189–205.
doi:10.2514/1.T3917
[22] Elkins, B., Keyhani, M., and Frankel, J. I., "Surface Heat Flux Prediction Through Physics-Based Calibration—Part 2: Experimental Verification," *AIAA Journal of Thermophysics and Heat Transfer*, Vol. 27, No. 2, 2013, pp. 206–216.
doi:10.2514/1.T3918
[23] Frankel, J. I., and Keyhani, M., "Nonlinear Inverse Calibration Heat Conduction Through Property Physics," *AIAA Journal of Thermophysics and Heat Transfer*, Vol. 28, No. 2, 2014, pp. 203–217.
doi:10.2514/1.T4269
[24] Frankel, J. I., and Keyhani, M., "Phase-Plane Analysis and Cross-Correlation for Estimating Optimal Regularization Parameters in Inverse Heat Conduction Problems," *AIAA Journal of Thermophysics and Heat Transfer*, Vol. 28, No. 3, 2014, pp. 542–548.
doi:10.2514/1.T4357
[25] Frankel, J. I., and Keyhani, M., "Cross Correlation and Inverse Heat Conduction by a Calibration Method," *AIAA Journal of Thermophysics and Heat Transfer*, Vol. 31, No. 3, 2017, pp. 746–756.
doi:10.2514/1.T5059
[26] Frankel, J. I., Chen, H. C., and Keyhani, M., "New Step Response Formulation for Inverse Heat Conduction," *AIAA Journal of Thermophysics and Heat Transfer*, Vol. 31, No. 4, 2017, pp. 989–996.
doi:10.2514/1.T5067
[27] Loehle, S., Battaglia, J. L., Batsale, J. C., Bourserau, F., Conte, D., Jullien, P., Ootegem, B. V., Couzi, J., and Lasserre, J. P., "Estimation of High Heat Flux in Supersonic Plasma Flows," *IECON 2006—32nd Annual Conference on IEEE Industrial Electronics*, Vol. 4, IEEE, New York, 2006, pp. 5366–5373.
doi:10.1109/IECON.2006.347752
[28] Loehle, S., Battaglia, J. L., Jullien, P., Ootegem, B. V., Couzi, J., and Lasserre, J.P., "Improvement of High Heat Flux Measurement Using a Null Point Calorimeter," *AIAA Journal of Spacecraft and Rocket*, Vol. 45, No. 1, 2008, pp. 76–81.
doi:10.2514/1.30092
[29] Loehle, S., and Frankel, J. I., "Physical Insight into System Identification Parameters Applied to Inverse Heat Conduction Problems," *AIAA 50th AIAA Aerospace Sciences Meeting and Exhibit*, AIAA Paper 2012-0809, Jan. 2012.
[30] Ozisik, M.N., *Heat Conduction*, Wiley, New York, 1980, Chaps. 1–3.
[31] Kidd, C. T., "High Heat Flux Measurements and Experimental Calibrations Characterizations," *The 1992 NASA Langley Measurement Technology Conference: Measurement Technology for Aerospace Applications in High-Temperature Environments*, NASA Langley, Hampton, VA, 1992, pp. 31–50.
[32] Powars, C. A., Kennedy, W. S., and Rindal, R. A., "Heat Flux Measurement Using Swept Null Point Calorimetry," *Journal of Spacecraft and Rockets*, Vol. 9, No. 9, 1972, pp. 668–672.
doi:10.2514/3.61773
[33] Woodbury, K. A., "Effect of Thermocouple Sensor Dynamics on Surface Heat Flux Predictions Obtained via Inverse Heat Transfer Analysis," *International Journal of Heat and Mass Transfer*, Vol. 33, No. 12, 1990, pp. 2641–2649.
doi:10.1016/0017-9310(90)90200-E
[34] Frankel, J. I., Elkins, B. E., and Keyhani, M., "Rate-Based Sensing Concepts for Heat Flux and Property Estimation; and, Transition Detection," *16th AIAA/DLR/DGLR International Space Planes and Hypersonic Systems and Technologies Conference*, AIAA Paper 2009-7303, 2009.
[35] Kinnear, K. M., and Lu, F. K., "Design, Calibration and Testing of Transient Thin Film Heat Transfer Gauges," *20th AIAA Advanced Measurement and Ground Testing Technology Conference*, AIAA Paper 1998-2504, 1998.
[36] George, W. K., Rae, W. J., and Woodward, S. H., "An Evaluation for Analog and Numerical Techniques for Unsteady Heat Transfer Measurements with Thin-Film Gauges in Transient Facilities," *Experimental Thermal and Fluid Science*, Vol. 4, No. 3, 1991, pp. 333–342.
doi:10.1016/0894-1777(91)90050-2
[37] Bertolazzi, E., Battisti, L., and Trivellato, F., "Numerical Processing of Thin-Film Thermometer Data for Determining Transient Heat Fluxes," *Applied Mathematical Modelling*, Vol. 36, No. 8, 2012, pp. 3645–3662.
doi:10.1016/j.apm.2011.09.089
[38] Keltner, N. R., Bainbridge, B. L., and Beck, J. V., "Rectangular Heat Source on a Semi-Infinite Solid—An Analysis for a Thin Film Heat Flux Gage Calibration," *Journal of Heat Transfer*, Vol. 110, No. 1, 1988, pp. 42–48.
doi:10.1115/1.3250470
[39] Irimpan, K. J., Mannil, N., Arya, H., and Menezes, V., "Performance Evaluation of Coaxial Thermocouple Against Platinum Thin Film Gauge for Heat Flux Measurement in Shock Tunnel," *Measurement*, Vol. 61, Feb. 2015, pp. 291–298.
doi:10.1016/j.measurement.2014.10.056
[40] Flaherty, W., and Austin, J. M., "Comparative Surface Heat Transfer Measurements in Hypervelocity Flow," *Journal of Thermophysics and Heat Transfer*, Vol. 25, No. 1, 2011, pp. 180–183.
doi:10.2514/1.50450
[41] Sneddon, I. N., *Fourier Transforms*, Dover, New York, 1995, p. 17.
[42] Linz, P., *Analytical and Numerical Methods for Volterra Equations*, SIAM, Philadelphia, 1985, pp. 165–175.
[43] Cook, W. J., and Felderman, E. J., "Reduction of Data from Thin Film Heat Transfer Gauges: A Concise Numerical Technique," *AIAA Journal*, Vol. 4, No. 3, 1966, pp. 561–562.
doi:10.2514/3.3486
[44] Sanderson, S. R., and Sturtevant, B., "Transient Heat Flux Measurement Using a Surface Junction Measurement," *Review of Scientific Instruments*, Vol. 73, No. 7, 2002, pp. 2781–2787.
doi:10.1063/1.1484255
[45] Piccini, E, Guo, S. M., and Jones, T. V., "The Development of a New Direct-Heat-Flux Gauge for Heat-Transfer Facilities," *Measurement Science and Technology*, Vol. 11, No. 4, 2000, pp. 342–349.
doi:10.1088/0957-0233/11/4/302
[46] Abramowitz, M., and Stegun, I. A., *Handbook of Mathematical Functions*, Dover, New York, 1972, pp. 1019–1030.
[47] Frankel, J. I., and Chen, H. C., "Heat Flux Data Reduction Using a Natural Filter Test Function," *AIAA SciTech Forum*, AIAA Paper 2019-1553, Jan. 2019.
[48] Frankel, J. I., "Regularization of Inverse Heat Conduction by Combination of Rate Sensors Analysis and Analytic Continuation," *Journal of Engineering Mathematics*, Vol. 57, No. 2, 2007, pp. 181–198.
doi:10.1007/s10665-006-9073-y
[49] Lamm, P. K., "A Survey of Regularization Methods for First-Kind Volterra Equations," *Surveys on Solution Methods for Inverse Problems*, edited by D. Colton, H. W. Engl, A. Louis, J. R. McLaughlin, and W. Rundell, Springer, New York, 2000, pp. 53–82.
[50] Groetsch, C. W., "Differentiation of Approximately Specified Functions," *The American Mathematical Monthly*, Vol. 98, No. 9, 1991, pp. 847–850.
doi:10.1080/00029890.1991.12000802
[51] Hanke, M., and Scherzer, O., "Inverse Problems Light: Numerical Differentiation," *American Mathematical Monthly*, Vol. 108, No. 6, 2001, pp. 512–521.
doi:10.1080/00029890.2001.11919778
[52] Frankel, J. I., Chen, H. C., and Mathew, K., "Design-to-Validation of a New Heat Flux Source with Uncertainty Analysis," *AIAA Journal of Thermophysics and Heat Transfer*, Vol. 33, No. 2, 2019, pp. 517–535.
doi:10.2514/1.T5519